EGG-TMI-7784

TMI-2 REACTOR VESSEL LOWER HEAD HEATUP CALCULATIONS

Richard L. Moore

Published August 1987

EG&G Idaho, Inc.
Idaho Falls, Idaho 83415

Prepared for the
U.S. Department of Energy
Idaho Operations Office
Under DOE Contract No. DE-AC07-76ID01570

ABSTRACT

This report presents the results of a study to determine the thermal response of the TMI-2 reactor vessel lower head to various assumed debris configurations. Three different debris configurations were considered, namely, (a) control rod material adjacent to the vessel wall overlaid by porous core material, (b) solid core material adjacent to the vessel wall overlaid by porous core material, and, porous core material adjacent to the vessel wall. Each configuration was analyzed for a quenched and unquenched condition in the porous debris material. The results indicate that a wide range of vessel thermal responses are possible, based on the debris configuration and debris cooling assumptions.

CONTENTS

FIGURES

TABLES

TMI-2 REACTOR VESSEL LOWER HEAD HEATUP CALCULATIONS

1. INTRODUCTION

On March 28, 1979, the Three Mile Island Unit 2 (TMI-2) nuclear reactor experienced a small-break loss-of-coolant accident (LOCA). The accident eventually led to uncovery, rapid heatup, and degradation of the core, such that core material actually relocated to the lower plenum of the reactor, as confirmed by camera inspection of the lower plenum. Best estimates to date put the amount of core material in the lower plenum at between 10 and 20% (10000 to 20000 kg) of the core loading.[1]

Cronenberg, Behling, and Broughton[2] assessed potential damage to the lower head caused by thermal attack from the relocated core debris. However, they concentrated on potential damage to the instrument penetration tubes that penetrate the lower head of the reactor. The intent in this report is to present the calculations, and their results, to assess the thermal response of the vessel wall as a function of debris configuration, composition, and initial temperature. The results compliment those already presented in Reference 2.

It is not the intent in this report to discuss the events leading up to the relocation of the core material, nor the mechanisms that may have caused the core material to relocate to the lower head. These subjects have been covered elsewhere, namely References 3 and 4. Reference 3 presents a best-estimate scenario of the progression of core damage. It is based on physical evidence gathered during the TMI-2 defueling effort and on supporting analysis completed as of December 1986. This scenario may change as more information becomes available. Reference 4 discusses plausible thermal and mechanical failure mechanisms of the crust surrounding the noncoolable debris in the lower core region, which led to the relocation of the core material to the lower vessel head.

At present, relocation of molten core material to the lower plenum is thought to have occurred, owing to failure of the crust surrounding the molten core material located in the lower core region, shown in Figure 1.

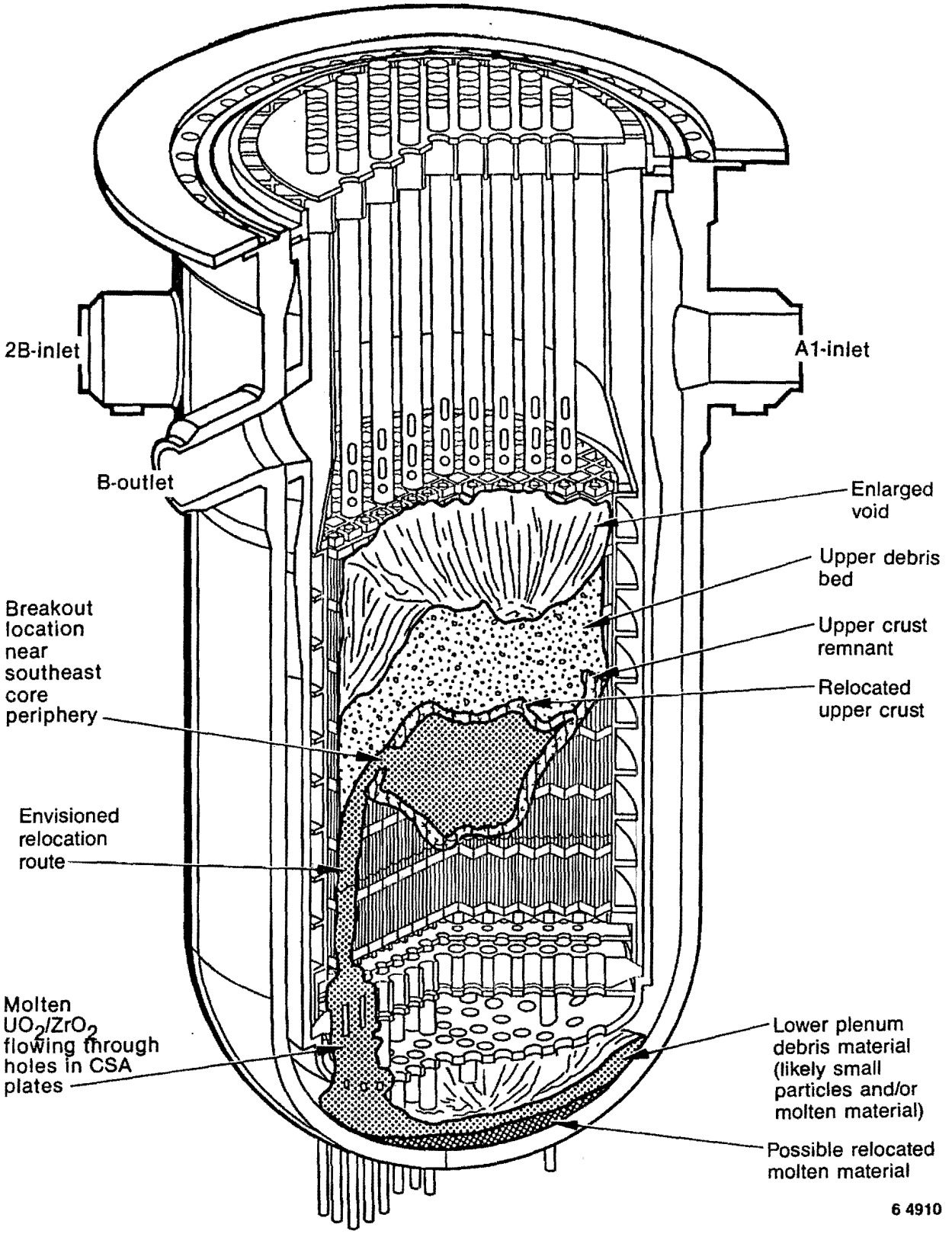

Figure 1. Hypothesized core damage configuration at 224 min (lower plenum relocation).

TMI-2 on-line data (neutron count rate at the source-range monitor, sudden increase in primary system pressure, and the simultaneous alarms of the self-powered neutron detectors) suggest that the molten core material may have relocated in about one minute. It is estimated that the coolant liquid level at time of relocation was above or near the top of the core.

2. COMPOSITION OF RELOCATED CORE MATERIAL AND CONFIGURATIONS MODELED

To assess the potential damage to the lower head by thermal attack from the relocated core material requires a knowledge of the composition of such material and its geometrical configuration.

Based on events recorded approximately 224 min into the accident, it is highly likely that molten core material relocated to the lower plenum during a short interval centered around the 224-min time frame. Postaccident examination of the TMI-2 reactor further reveals that the molten core material probably originated from near the top of the lower core blockage, owing to a break in the crust at the periphery of the blockage. Preliminary analysis of the blockage in the lower core region indicates that prior to this relocation approximately 12000 kg of core material in the blockage could have been molten.[4] At these high temperatures, convection currents in the melt should have developed, thus providing a homogeneous-like mixture of UO_2, Zr, ZrO_2, and some control rod material (silver-indium-cadmium).

Postaccident visual inspection of the lower plenum indicates that most of the molten core mixture relocated to the lower plenum. Examination of the loose debris from the lower plenum (top surface of the debris) indicates the relocated material is composed primarily of ceramic fuel (UO_2) and cladding (Zr).[5] It is assumed for the analysis presented in this report that the core material in the lower plenum is a homogenized mixture, 80 and 20 percent by mass of UO_2 and Zr. The effects of control rod material on the thermal properties of the mixture have been neglected for this analysis; however, if more extensive sampling of the lower plenum debris should show significant amounts of control rod material in the debris its effect will have to be accounted for in later analyses.

The specific location of the greater part of the control rod material has not yet been identified. The question of control rod material location arises from examination of the gamma-scanning data obtained via insertion of a thin-tube ion chamber in the single open penetration tube (L-U).[6,7]

The findings differ from what would be expected if a layer of U-Zr-O ceramic existed at the bottom of the plenum. The data show the activity of fission products increased with increased height above the lower head, suggesting a nonfuel layer of material approximately 9 in. in height at the centerline of the reactor.[2] At present, it is difficult to assess how much control rod material is contained in the relocated core material. The control rod material has a melting temperature of approximately 1100 K. With such a low melting temperature, it is likely that control rod material was the first material, along with its stainless steel cladding, to reach melting temperature and relocate to the lower core region, thus forming the initial lower core blockage. Later, high-temperature molten fuel and zircaloy cladding relocated on top of the control rod material. At this point, one can only speculate as to what happened to the control rod material. One possible scenario is that the control rod material remelted from the heat of the material above it, and, thus, relocated to the lower plenum prior to the massive core material relocation. Such relocation would have involved relatively small amounts of material, thus producing small fragments that would have been totally quenched by the time the control rod material reached the lower head. A second scenario assumes that the control rod material stayed in the lower core region, remelted, with most of it mixing and remaining in the lower region of the molten pool. In a convecting molten pool, experimental evidence indicates that the heat transfer from the bottom of the molten pool behaves as though the heat is being conducted, rather than convected, from the molten pool.[8] This implies that convective motion is negligible or absent in the lower pool region. If this is the case, the more dense control rod material may not have mixed with the molten fuel but remained at the bottom of the molten lower core pool.

Based on the uncertainties of the configuration and composition of material in the lower plenum, as well as the quenchability of the relocated material, six cases were considered to bound the thermal response of the vessel wall. Case 1 consists of a 7.7-in.-thick (0.196-m- at reactor centerline) layer of nonfuel material (control rod-like material; porosity = 0) initially at 559 K, overlaid with a layer of heat-generating porous U-Zr-O ceramic (porosity = 0.65) initially at 2500 K, as shown in

Figure 2. This layer of control rod material represents 70% of the original control rod material. For this case, we assume that the porous debris material quenches within 20 min. Case 2 is the same as Case 1, except that we assume the porous debris is unquenchable. The porous layer is assumed to be 16.3 in. (0.414 m) high, which yields an overall height of relocated material of 24.0 in. (0.610 m). The total height of 24 in. is the same for all cases considered. Case 3 is a mixture of heat-generating U-Zr-O ceramic (no porosity) initially at 2500 K, overlaid with a porous layer of U-Zr-O (porosity = .65) initially at a temperature of 2500 K. We assume that the porous debris material quenches within 20 min from the time the bed formed. The height of the solid layer (control rod material for Cases 1 and 2, core material for Cases 3 and 4) is the same for all cases where it has been assumed that a solid layer of material lies adjacent to the lower head. Case 4 is the same as Case 3, with the exception that the porous debris is unquenchable. Case 5 assumes that the entire debris bed is porous (no solid region; porosity = .65) with an initial temperature of 2000 K. We assume that the debris bed is quenched within 20 min from the time of formation. Case 6 is the same as Case 5 except, again, we assume that the debris is unquenched during the transient considered.

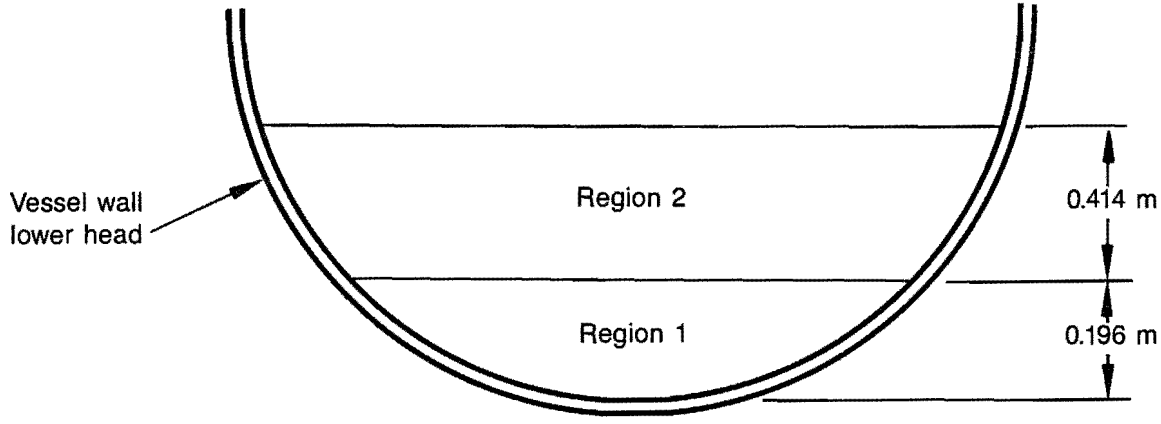

Cases	Region 1	Region 2
1 (Lower bound thermal response)	Control rod material (559K)	Fuel debris (2500K), quenched within 20 minutes
2 (Intermediate bound thermal response)	Control rod material (559K)	Fuel debris (2500), unquenched
3 (Intermediate bound thermal response)	Solid Fuel (2500K)	Fuel debris (2500K), quenched within 20 minutes
4 (Upper bound thermal response)	Solid Fuel (2000K)	Fuel debris (2500), unquenched
5 (Intermediate bound thermal response)	Fuel debris (2000K), quenched within 20 minutes	Fuel debris (2000K), quenched within 20 minutes
6 (Intermediate bound thermal response)	Fuel debris (2000K), unquenched	Fuel debris (2000K), unquenched

7-8520

Figure 2. Schematic showing the configurations considered in the analysis.

3. COUPLE MODEL OF THE LOWER PLENUM AND VESSEL WALL

The lower head and relocated core material were modeled using COUPLE/FLUID, a two-dimensional finite element transient heat conduction and advection code[9], where advection refers to the transport of energy by means of a flowing fluid. For the analysis presented in this report the code solves the following two-dimensional energy transport equation:

$$(\rho C)_e \frac{\partial T}{\partial t} = \nabla \cdot K\nabla T + Q \qquad (1)$$

where

$(\rho C)_e$ = $\phi\ (\rho C)_\ell + (1 - \phi)(\rho C)_s$

ρ = density (kg m^{-3})

C = specific heat (J kg^{-1} K^{-1})

k = thermal conductivity (w m^{-1} K^{-1})

Q = volumetric heat generation rate (w m^{-3})

T = temperature (K)

ϕ = porosity of solid material.

The subscripts are defined as follows:

e = equivalent

ℓ = liquid

s = solid.

Equation (1) is solved using Galerkin's weighted residual technique in conjunction with linear basic functions. This is a standard technique used to obtain approximate solutions to linear and nonlinear partial differential equations via the finite element method. The capability to model the freezing and/or melting of various reactor materials has been added to the code through the addition of several subroutines.

The numerical modeling of heat transfer in a region that is undergoing a change of phase (freezing or melting) is more difficult than modeling a nonphase change region. This is due to the changing location of the interface between liquid and solid region as a function of time, dependent on the development of the transient temperature field. In addition, the local liberation of latent heat may cause a significant heat flux discontinuity at the phase boundary.

At present, there are two generally accepted ways of numerically approximating a phase change problem. One method uses a moving mesh technique; the other method uses a fixed mesh technique. At this time, the moving mesh technique is primarily used to solve one-dimensional problems. The moving mesh technique is not easily adapted to two-dimensional problems, owing to its tendency to cause mesh distortion. Thus, we have chosen a fixed mesh technique to model the phase change in the debris. The particular method we have chosen is described in Reference 10. The method consists of using the material enthalpy to determine an effective density time specific heat ($\rho\ C_p$) value to use in Equation (1). The enthalpy per unit volume is defined as

$$H = \int \rho\ C_p\ dT \tag{2}$$

thus

$$\rho C_p = dH/dT \tag{3}$$

which can be written as

$$\rho C_p = \frac{dH}{dX}\frac{dX}{dT} \qquad (4)$$

where

$\frac{dH}{dX}$ = enthalpy gradient normal to phase change interface

$\frac{dX}{dT}$ = inverst of the temperature gradient normal to the phase change interface.

For computation, it is easier to calculate dH/dX and dX/dT than it is dH/dT directly. Using the enthalpy approach, a local discontinuity such as an enthalpy jump at the phase change boundary will automatically be accounted for, since the enthalpy of any material is a monotonically increasing function of temperature.

3.1 Lower Head Configuration Model

The lower head of the TMI-2 reactor consists of a 5-in.-thick carbon steel wall in the shape of a hemisphere. The inside radius of the hemisphere is 2.215 m. The lower head inside surface is covered with a thin layer of stainless steel (3/8 in. thick). The outside surface of the lower head is assumed to be shielded from the external environment by a thin stainless steel radiation shield. For ease of modeling, it has been assumed that the top surface of the core material in the lower plenum forms a level surface in the horizontal plane. The total height of the relocated core material was assumed to be 0.6 meters at the centerline of the reactor, as measured from the inside surface of the vessel wall. The height of the solid layer of material for Cases 1, 2, 3, and 4 was assumed to be approximately 0.2-meters high at the centerline of the reactor.

The finite element mesh developed for this analysis is shown in Figures 3 and 4. Figure 3 displays the node numbers associated with the

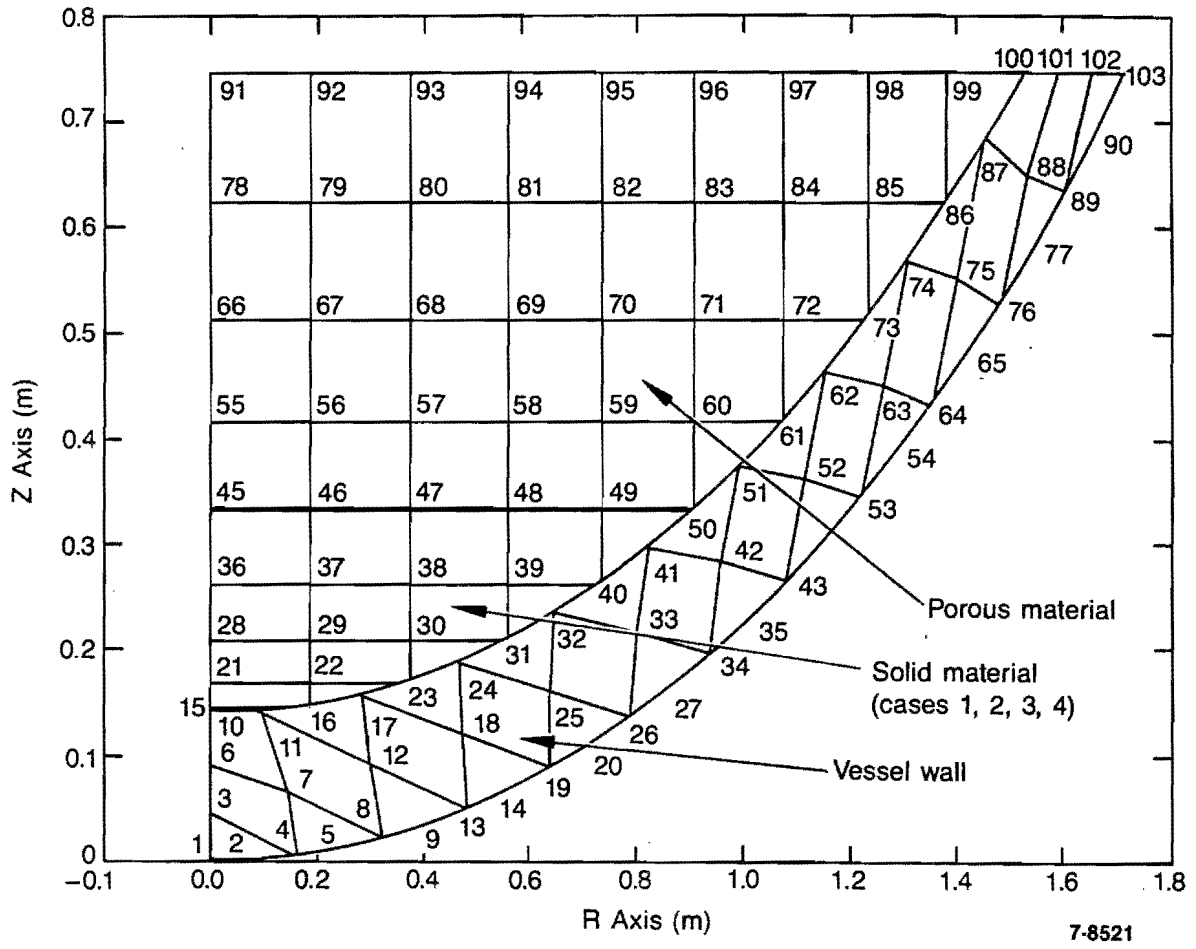

Figure 3. Node numbers.

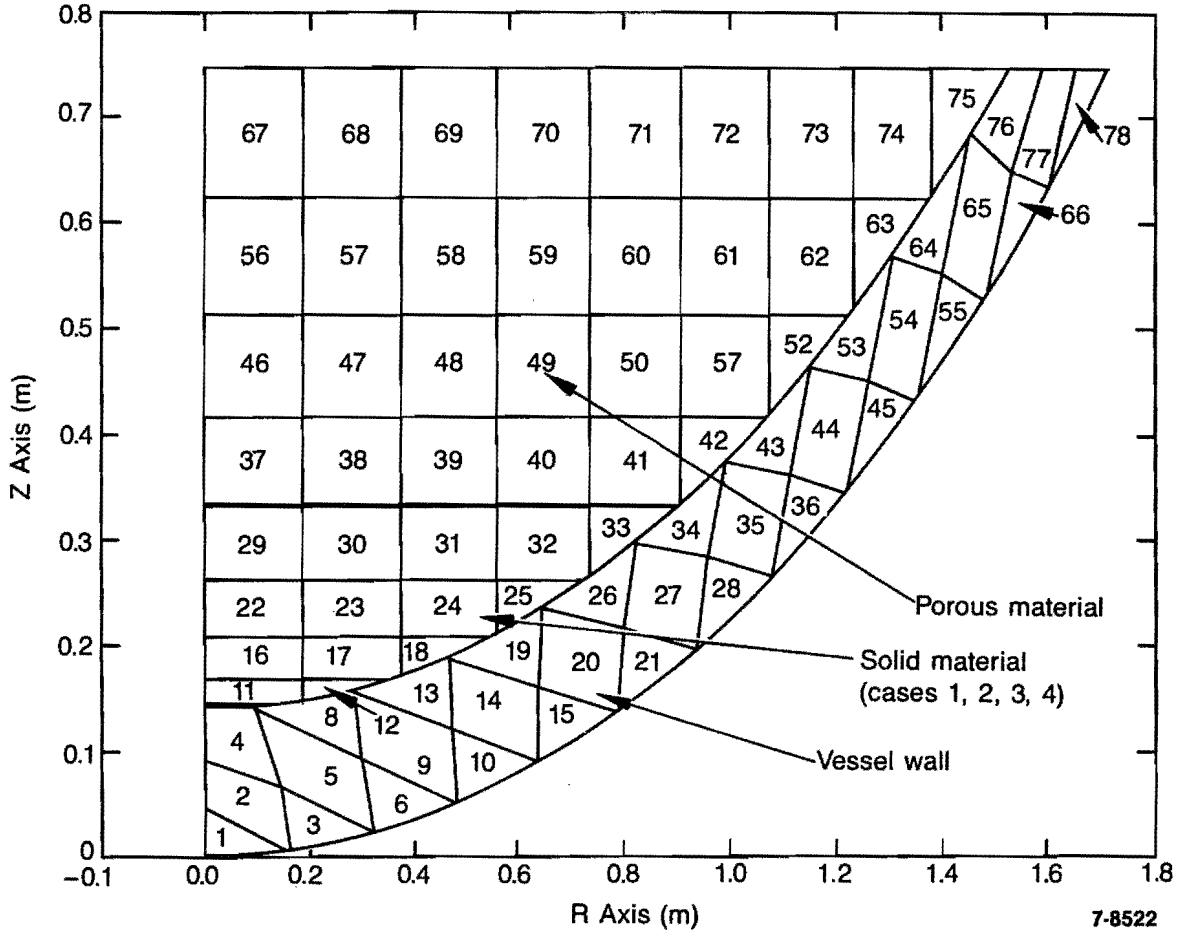

Figure 4. Element numbers.

mesh, whereas Figure 4 contains the element numbers associated with each element of the model. The model was developed using cylindrical coordinates. Axial-symmetry was also assumed about the reactor centerline. The lower head vessel wall is represented by the elements lying between the two curved lines in Figure 4. The thin stainless liner has been construed as part of the vessel wall. This was done for ease of modeling, and will have no noticeable effect on the predicted temperatures.

3.2 Boundary Conditions

In order to predict the transient temperature history of the lower plenum vessel wall, as well as the relocated core material, several boundary conditions are needed. As the outer surface temperature of the reactor vessel wall increases above the containment temperature, energy is transferred from the wall to the containment environment by means of convection and radiation. For this analysis, the outer surface of the lower head is assumed to radiate to a thin stainless steel shield, which in turn radiates and convects to the containment environment. Effective radiation and convective heat transfer coefficients were calculated and applied between the outer surface of the lower head and a 311-K sink temperature used to represent the external environment. The initial temperature of the reactor vessel wall was assumed to be 559 K, corresponding to the coolant saturation temperature at a pressure of 7.0 MPa.

Thermal boundary conditions are also necessary to simulate the environment surrounding the relocated core material. For this study, we assume that the top surface of the debris immediately quenches to 559 K. This condition is used to simulate nucleate boiling along the top of the debris bed and results in the removal of the maximum amount of heat possible from the top of the heat-generating debris bed. In the model, this is simulated by constraining the top surface of the debris bed to be 559 K and holding the surface at the constrained temperature for the duration of the transient considered. We have also assumed for some of the cases that the porous debris bed will become completely quenched sometime during the transient.

From recent TMI-2 debris coolability studies,[11] it has been estimated that it will require approximately 20 min to quench a debris bed of the size similar to the one produced in TMI. How the quench front will propagate is an unknown parameter; however, for our analysis we assume the following: since the lower head wall is cool relative to the debris material, we will assume that water penetrates the debris bed adjacent to the vessel wall and quenches radially from the vessel wall inward toward the reactor centerline. This gives us some insight as to how the vessel wall will respond thermally for quenched and unquenched debris configurations.

The position of the quench front was calculated by assuming that the area swept out by the quench front was constant in time and was independent of the vertical coordinate. In equation form, we have

$$V_o \pi r_o = V \pi r \tag{5}$$

where

V_o = initial quench velocity (m sec^{-1})

r_o = outer debris radius (m)

V = instantaneous quench front velocity (m sec^{-1})

r = position of quench front (m).

The time rate of change of the quench front is equal to the velocity of the quench front.

$$\frac{dr}{dt} = -V \tag{6}$$

Solving for V, using Equation (5), and substituting into Equation (6) yields

$$\frac{dr}{dt} = \frac{-V_o r_o}{r} \quad . \tag{7}$$

Integrating Equation (7) we have the quench front position as a function of time

$$r = \left(-2V_o\, r_o\, t + r_o^2\right)^{1/2} \tag{8}$$

The initial quench velocity is given by

$$V_o = \frac{r_o}{2t} \tag{9}$$

where t is the total quench time (20 min).

Table 1 presents the time of quench for the nodes in the porous core material. When the quench front is calculated to coincide with a node, that nodal temperature is decreased from 2500 to 559 K and held at 559 K until the end of the transient.

3.3 Thermal Properties

The thermal properties used for the analysis were obtained from MATPRO,[12] a data base for LWR material properties. Given the atomic fraction of each component of the mixture, the MATPRO thermal property package will return mixture density, specific heat, enthalpy, and thermal conductivity values. The mixture thermal conductivity values calculated by MATPRO were replaced by values calculated internal to the code. The approach used was to calculate two thermal conductivity values for the mixture (one based on a series model, the other based on a parallel model) and average these values to obtain the overall mixture thermal conductivity. The two models used are

TABLE 1. RADIAL QUENCH POSITION AS A FUNCTION OF TIME
(See Figure 2 for presentation of nodes.)

Time (Sec)	Nodes	Radius (meter)
0.0	100	1.526
109.6	87	1.456
211.5	86	1.385
315.7	74	1.310
473.9	85, 73	1.234
512.6	62	1.155
667.0	84, 72, 61	1.075
693.6	51	0.9913
829.6	83, 71, 60, 50	0.9077
962.9	82, 70, 59, 49	0.7341
1066.7	81, 69, 58, 48	0.5552
1140.7	80, 68, 57, 47	0.3723
1185.2	79, 67, 56, 46	0.1868
1200.0	78, 66, 55, 45	0.0

$$k_{T1} = \sum_{i}^{n} f_i \, k_i \tag{10}$$

and

$$\frac{1}{k_{T2}} = \sum_{i}^{n} f_i \, k_i \tag{11}$$

where

f_i = component mass fraction

k_i = component thermal conductivity.

The mixture conductivity without considering the effect of porosity becomes

$$k_{mix} = (k_{T1} + k_{T2})/2.0 \quad . \tag{12}$$

To obtain the overall mixture thermal conductivity, we now consider the effect of porosity on the debris material conductivity. The heat transfer in a dry porous bed involves both conduction and radiation. The overall thermal conductivity of the bed can be represented as

$$k_{et} = k_{ec} + k_r \tag{13}$$

where

k_{et} = total effective conductivity

k_{ec} = effective conductivity (conduction only)

k_r = radiation conductivity.

There have been a number of thermal conductivity models proposed for modeling a dry porous bed. Reference 13 gives a good review and comparison of five such models. As a result of their comparison, it appears that the Imura-Takegoshi[14] model combined with Vortmeyer's[15] radiation model yields the best overall results as far as providing an upper bound.

The Imura-Takegoshi model in equation form is given as follows:

$$k_{ec} = \psi + \frac{1 - \psi}{\delta + \frac{1 - \delta}{\nu}} \tag{14}$$

$$\delta = 0.3\, p^{1.6}\, \nu^{-0.44} \tag{15}$$

$$\nu = k_s/k_g \tag{16}$$

$$\psi = \frac{\phi - \delta}{1 - \delta} \tag{17}$$

where

k_g = gas or vapor thermal conductivity

k_s = k_{mix} = solid thermal conductivity

ϕ = porosity.

The Vortmeyer radiation model is given as

$$kr = 4\, \eta\, \sigma\, DT^3 \tag{18}$$

where

η = radiation exchange factor (1.0)

σ = Stefan-Boltzman constant (5.67×10^{-8} w m^{-2} K^{-4})

D = particle diameter (0.0127 m)

T = temperature.

The combined Imura-Takegoshi and Vortmeyer model was input into the COUPLE/FLUID code. The coding was checked out by comparing computer printout of the calculated effective thermal conductivity with hand calculations. This same model is used by Sandia in their MELPROG code.[16]

3.4 Decay Heating Rates

Total reactor core decay heating rate has been calculated previously.[17] This decay heating rate is shown in Table 2 and was used in this analysis to compute the power density of the heat generating materials. The total heating rates are shown both as a function of time and volatile fission product release fraction.

The COUPLE/FLUID code requires internal heat generation rates per unit volume (power density). Since we have a mixture of heat generating fuel and nongenerating cladding, the heating rate per unit volume depends on the fuel content of the volume. The power density in the core material is given by

$$P = (f)\ \rho(P_0/M_0)(1 - \phi) \tag{19}$$

where

P = power density of core material ($w\ m^{-3}$)

f = mass fraction of UO_2 in the mixture

ρ = mixture density ($kg\ m^{-3}$)

P_0 = total core decay power (w)

M_o = total mass of UO_2 in the core (93100 kg)

ϕ = porosity.

For this analysis, we assume a volatile fission product release fraction of 0.5, which is consistent with that used in the calculations presented in Reference 17. As indicated in Reference 17, the actual release fractions have not yet been determined; thus, the use of 0.5 is only an estimate of the real value. The use of 0.5 equates into a total core power of 20.0 MW at 224 min. The core power at 360 and 600 min are 18.2 and 14.8 MW, respectively. Equation 20 is then used to generate the appropriate power densities needed by the code.

TABLE 2. TMI-2 REACTOR CORE DECAY HEAT POWER (MW)

Time (h)	Volatile Fission Product Release Fraction					
	0.0	0.1	0.3	0.5	0.9	1.0
1	36.1	35.0	32.9	30.8	26.5	25.4
2	28.2	27.4	25.8	24.2	21.0	20.0
3	24.5	23.9	22.6	21.4	18.9	18.3
4	22.3	21.8	20.7	19.6	17.4	16.9
5	20.7	20.2	19.2	18.2	16.3	15.8
10	16.7	16.3	15.6	14.8	13.4	13.0
24	12.5	12.3	11.9	11.4	10.6	10.4

4. CREEP RUPTURE FAILURE

When hot debris material comes in contact with the lower head, the head will either survive, fail because of melt through, or fail because of creep rupture.

Failure caused by creep rupture can be determined using the Larson-Miller criterion. The time to rupture at a specified set of conditions for A-508, Class 2 carbon steel, is given as

$$t = 10^{(PLM/T - 20)} \tag{20}$$

where

t = time to failure (hr)

PLM = Larson-Miller parameter

T = material temperature (^{o}R).

For A-508, Class 2 carbon steel, the Larson-Miller parameter is

$$PLM = (-9603.0)(\log \sigma) + 46454.0 \tag{21}$$

where

$$\sigma = \frac{Pr}{2h} \tag{22}$$

and

P = system pressure (ksi)

r = inside radius of vessel

h = thickness of vessel wall

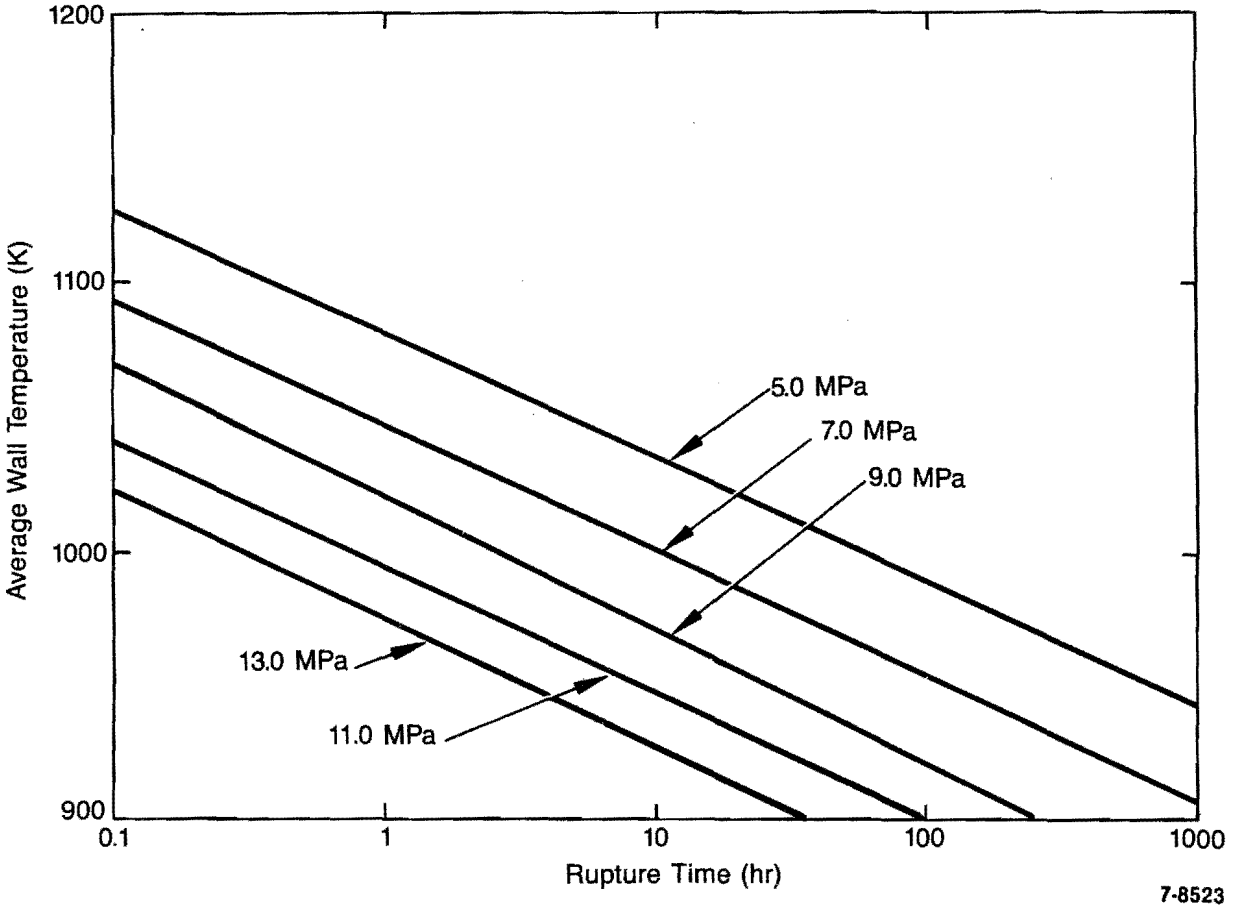

Figure 5. Average wall temperature versus rupture time for a carbon steel RPV lower head subjected to system pressures.

σ = stress (ksi).

A plot of rupture time versus average wall temperature for five different system pressures is presented in Figure 5. The importance of temperature relative to creep rupture of the vessel is easily observed from the Figure. For example, if the lower head is at an average temperature of 1000 K with a pressure differential across the vessel wall of 7 MPa we can expect the lower head to fail within 10 hours, owing to creep rupture. However, if the vessel wall is maintained at an average temperature of 1100 K results presented in Figure 5 indicate that the vessel wall will fail within 0.1 hours from the time the wall average temperature exceeds 1100 K.

Figure 5 illustrates the dramatic effect the wall temperature has on the predicted time to creep rupture failure of the reactor primary vessel lower head. There is one main limitation to the use of Figure 5 in the prediction of creep rupture failure--the use of an average wall temperature profile through the wall. To accurately predict the failure time associated with creep rupture would require a detailed finite element stress analysis; however, the rupture times shown in Figure 5 should give a reasonable estimate of the true rupture times.

5. CALCULATED VESSEL THERMAL RESPONSE

The results presented in this section show the temperature history of a few selected locations in the model (nodes; see Figure 3) which represent the lower head and debris material. For this study, we are mainly interested in the spatial thermal response of the lower head for the six cases described at the outset.

Figures 6, 7, 8, and 9 depict the temperature history of nodes 3, 25, 42, and 63 (see Figure 3 for node locations) for the six cases considered in this study. Nodes 3, 25, 42, and 63 represent four locations in the reactor vessel lower head of the TMI-2 reactor. Node 3 is located at the very bottom of the reactor at the midplane of the vessel wall. Node 42 represents a location in the midplane of the vessel wall adjacent to the location where the control rod material, the porous debris material, and the vessel wall coincide. Node 25 represents a vessel wall location approximately halfway between nodes 3 and 42. Node 63 represents a vessel wall location between node 42 and the upper surface of the debris.

Use Table 3 to identify each case presented in the figures. The identifier quenched or unquenched refers to the debris material lying above the solid layer of material, except for Cases 5 and 6 where we have all porous material. For Case 5, all the porous material is assumed to quench in 20 min.

The nomenclature at the top of each figure identifies the initial temperature of the various materials. The control rod material is assumed to have an initial temperature of 559 K [C(559)], the solid fuel material an initial temperature of 2500 K [SF(2500)], and the porous material for Cases 5 and 6 an initial temperature of 2000 K [PF(2000)]. The porous debris material lying on top of the solid layer for Cases 1, 2, 3, and 4 is assumed to have an initial temperature of 2500 K.

As previously shown, vessel wall failure at high internal pressures is predicted to occur within minutes (owing to creep rupture) when the average vessel wall temperature exceeds 1100 K. Carbon steel (vessel wall

TABLE 3. DESCRIPTION OF CASES

Case	Identifier	
1	—..—	Control rod material, quenched
2	———	Control rod material, unquenched
3	—-—-—	Solid fuel, quenched
4	—.—	Solid fuel, unquenched
5	—-—-—	Porous fuel, quenched
6	—.—	Porous fuel, unquenched

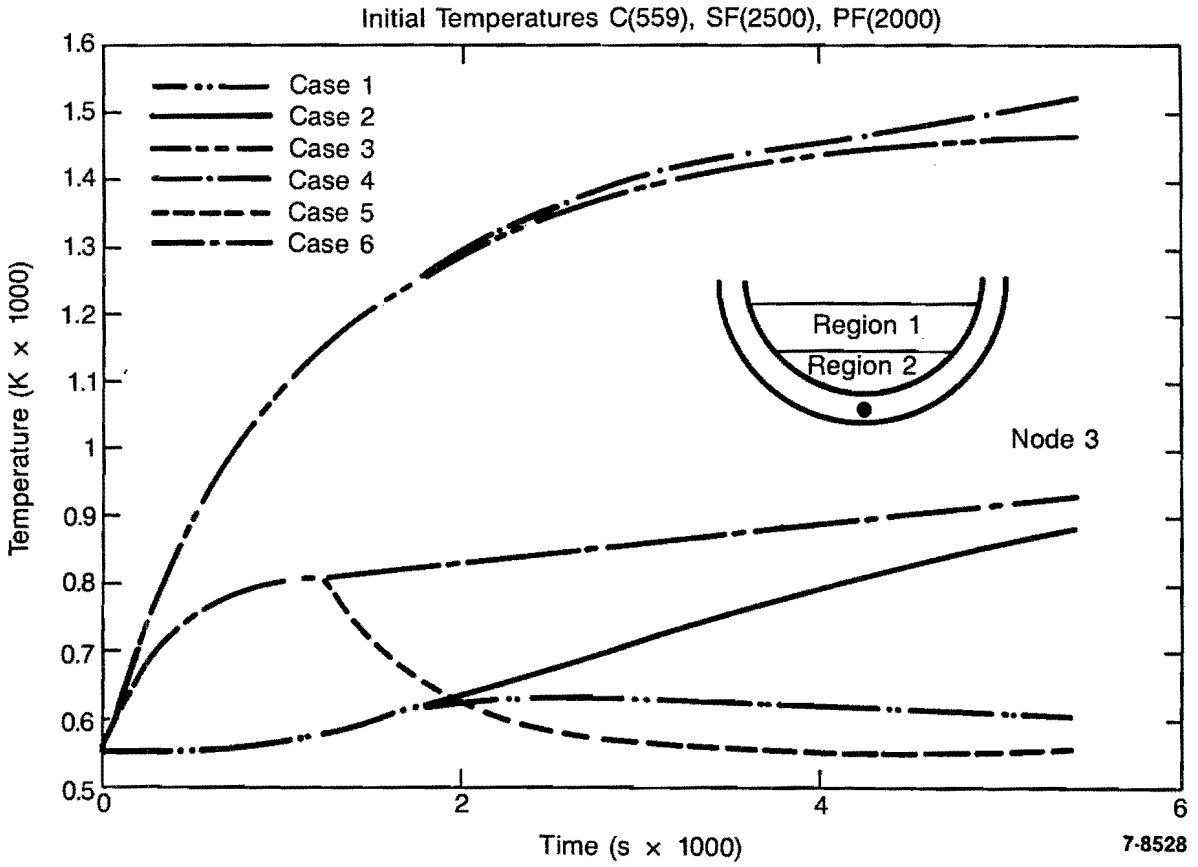

Figure 6. Temperature history of vessel wall node 3.

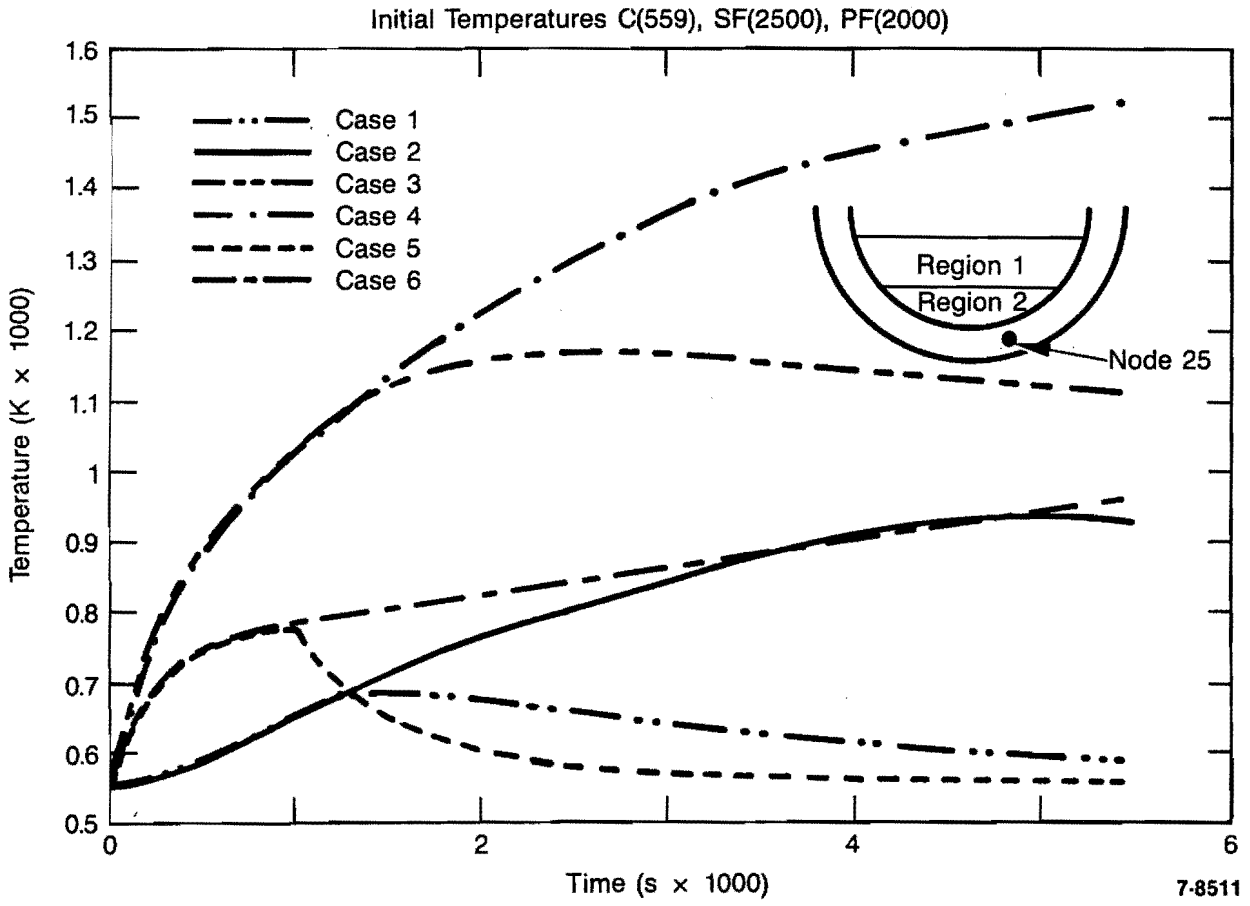

Figure 7. Temperature history of vessel wall node 25.

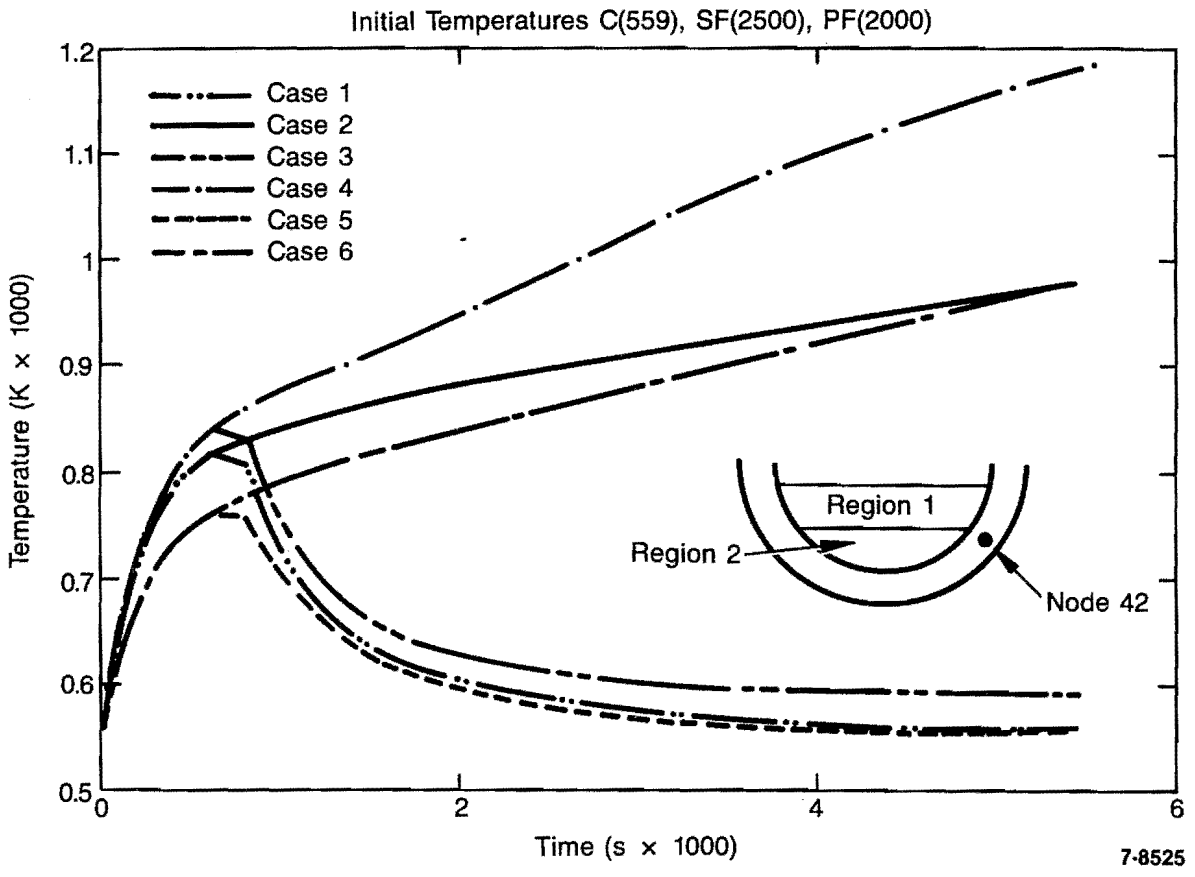

Figure 8. Temperature history of vessel wall node 42.

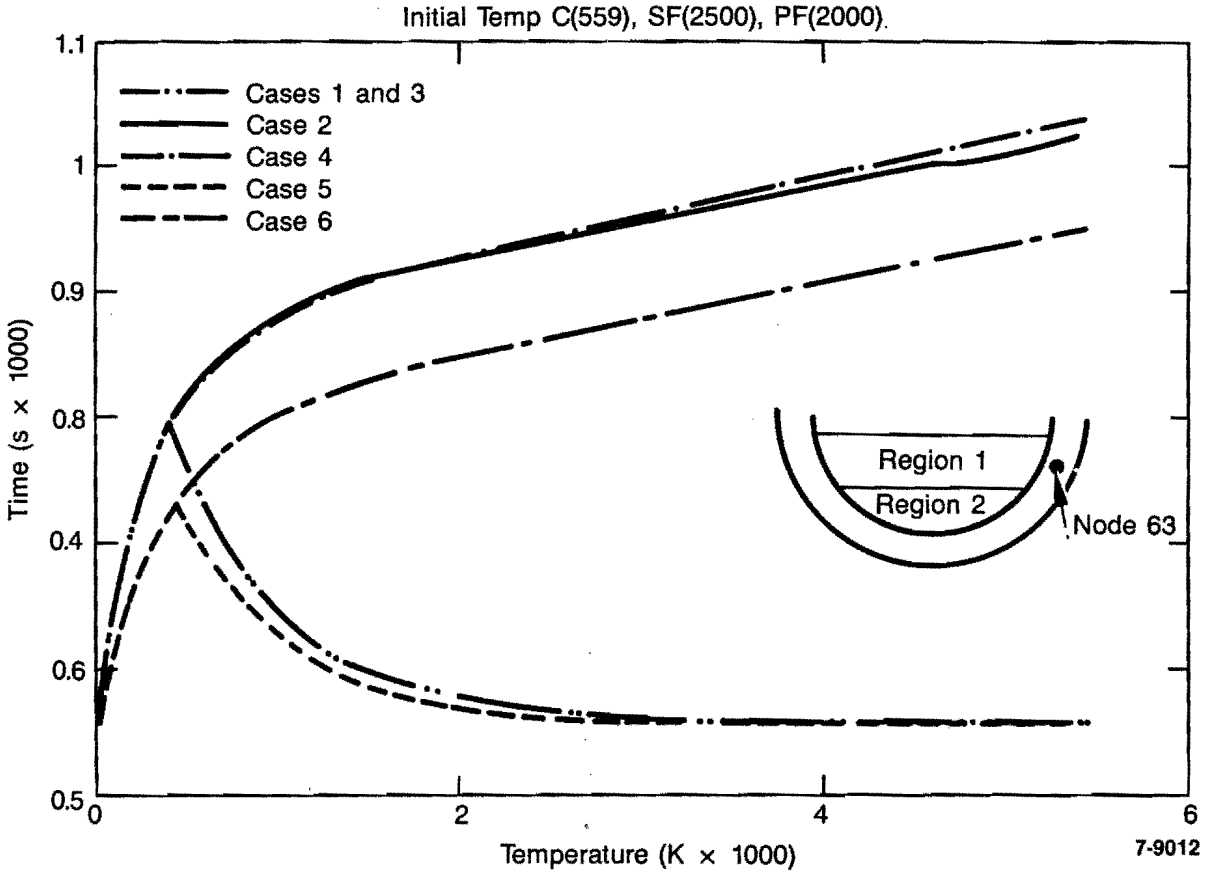

Figure 9. Temperature history of vessel wall node 63.

material) begins to melt around 1650 K; thus, it is likely the reactor vessel wall will fail as a result of creep rupture rather than melting. For this reason, we have chosen to present mid-wall temperature histories, which are assumed to represent the vessel wall average temperature. At the time peak mid-wall temperatures occur, the temperature profile through the wall is approximately linear; thus, the assumption that the mid-wall temperature represents the average wall temperature is reasonable for the scoping type calculation in this report. A table summarizing our analysis of the cases is presented later, wherein the maximum vessel wall temperature and peak average wall temperature are shown.

For Case 1, we see from Figures 6, 7, 8, and 9 that the inner vessel wall just below the control rod material debris interface (node 42) experiences the highest average temperature. Figure 8 shows the temperature of node 42 rising from 559 K to a peak temperature of 825 K at 680 s into the transient. From that point on, the temperature of node 42 decreases rapidly, owing to the assumed quench of the fuel debris. At 5400 s, the temperature of node 42 has dropped to 560 K. The rapid heatup of node 42 compared to the vessel locations beneath the control rod material (nodes 3 and 25) is due to the closeness of the high-temperature debris bed (initial temperature 2500). Thus, we clearly see that the peak average vessel wall temperature for an assumed layer of control rod material between the fuel debris and vessel is not sufficient to cause melting or creep rupture of the vessel.

Case 2 (same as Case 1 except no fuel debris quench) shows the peak average vessel wall temperature (node 63) to be at the vessel wall midplane, midway between the control rod material debris interface and the top of the debris. The temperature is seen to rapidly increase to 896 K by 1200 s, and then gradually increase to 1023 K by 5400 s. The rapid increase is due to the initial high-temperature debris material, whereas the gradual increase during the remainder of the transient is due to the gradual heatup (caused by decay heat) of the debris material. The temperature of the upper debris (node 68), which is driving the heat up the vessel wall, is shown in Figure 10. If the transient were carried beyond 5400 s with no cooling of the fuel debris, the peak average vessel wall

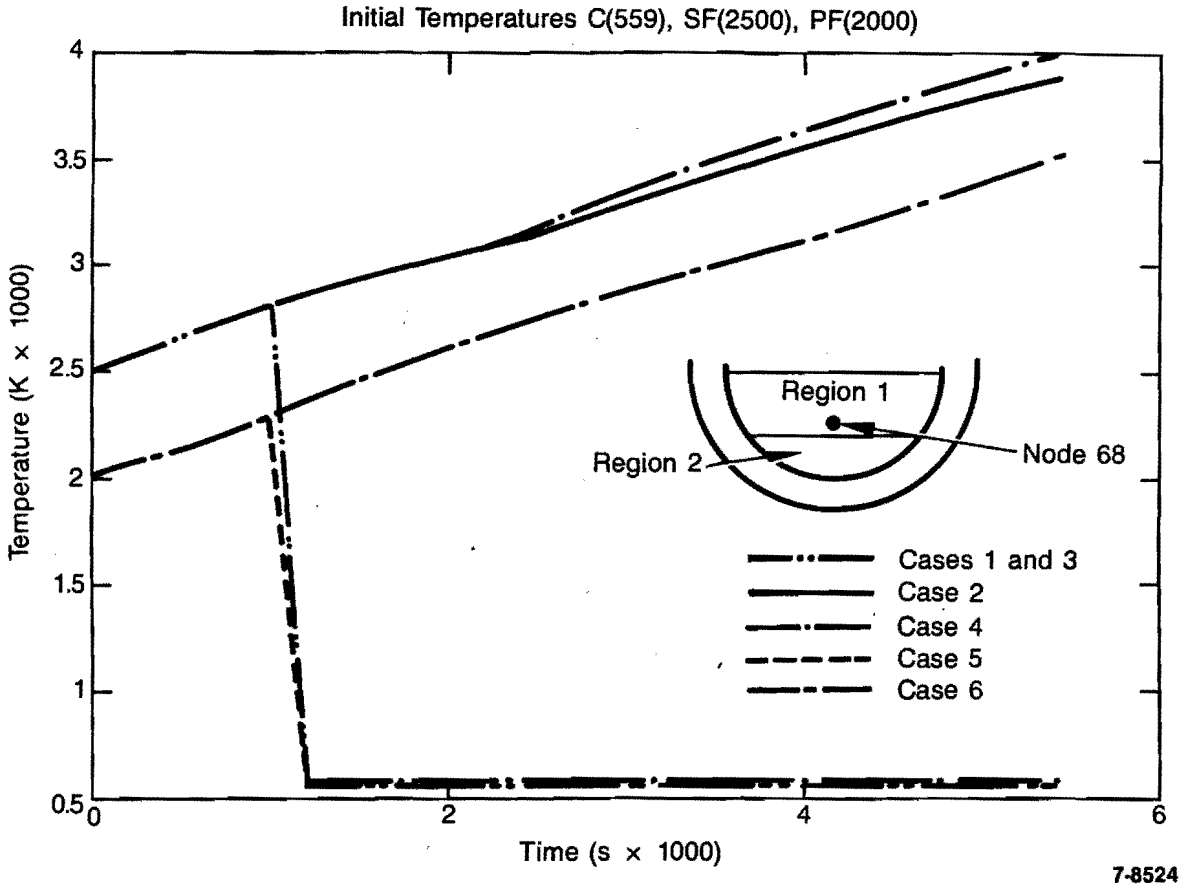

Figure 10. Temperature history of debris node 68.

temperature (node 63) would eventually exceed 1100 K and vessel failure caused by creep rupture would be possible. However, if the debris bed were to quench any time during the 5400 s transient the vessel peak average temperature (node 63) would immediately start to decrease, as indicated by the Case 1 calculation. Thus, the integrity of the vessel wall is seen to be a strong function of the fuel debris cooling.

In Case 3, the layer of control rod material is replaced by a layer of solid heat-generating U-Zr-O ceramic, and the debris layer above the solid layer is totally quenched 20 min after the start of the transient. For this case, the vessel peak average temperature occurred at the vessel wall midplane located on the reactor centerline (node 3). Figure 6 shows the peak average temperature of node 3 increasing from 559 to 1100 K within 1000 s after the start of the transient. The temperature continues to increase and reaches 1460 K at 5400 s. Using the Larson-Miller criterion, the reactor vessel is expected to fail at this temperature. The quenching of the upper debris bed has little effect on the calculated vessel temperatures. This is expected, since the vessel location (node 3) is relatively isolated from the effects of quenching the upper debris material. However, as seen in Figure 7, the quenching of the debris bed has a strong influence on the temperature history at the vessel mid-radius location (node 42).

Case 4 is the same as Case 3, except the debris bed is unquenched during the transient. Figure 6 shows very little difference in the calculated peak average vessel temperatures (node 3) between cases 3 and 4. Again this is due to the relative isolation of node 3 compared to nodes 25, 42, and 63. Toward the end of the transient, the temperature of node 3 for the quench case is slightly lower than for the unquenched case.

Cases 5 and 6 correspond to an all porous debris bed at an initial temperature of 2000 K, Case 5 being the quenched case, Case 6 the unquenched case. For the quenched case, node 3 reaches a maximum temperature of 800 K at 1200 s, and steadily decreases to 560 K at the end of the transient. For the unquenched case, node 42 reaches a maximum temperature of 974 K at the end of the 5400 s transient. Thus, a porous

unquenched debris bed could reside on the lower head for as long as 5400 s without fear of a lower head failure for the given conditions used in this analysis.

As stated earlier, Figure 10 presents the temperature history of node 68, which corresponds to a porous debris node (see Figure 3). Figure 11 shows the temperature history of node 38, which is used to represent the solid debris material. The sharp drop in temperature in these figures represents the quenching of the node. As indicated by the results presented in Figures 10 and 11, the porous debris region (unquenched case) and the solid fuel region (quenched and unquenched cases) both experience temperatures that exceed the melting temperature of UO_2 (~2850 K), thus, a convecting molten pool would likely develop. The effects on the results presented in this report of a convecting molten pool have been neglected for this study; however, comparing Figures 6 and 11 we see by the time the solid layer of fuel has reached a temperature of 2850 K (~2500 s) the average vessel wall temperature is predicted to be 1340 K. Thus, as indicated by Figure 5, the vessel wall would probably have failed owing to creep rupture long before any molten pool was created. If this were not the case, a convecting molten pool would tend to cause the vessel wall to heat up at a more rapid rate once the pool became highly convective.

Figures 12 and 13 present the mid-wall temperature profile (transient time = 1200 s) for the quenched and unquenched cases analyzed. The shape of the profiles are indicative of the assumptions used for each case. The control rod quenched case shows the vessel wall temperature increasing from 584 K at the axial centerline of the reactor to 701 K at the location where the control rod material, porous debris bed, and vessel wall intersect. The wall temperature then decreases to 564 K at the intersection of the top of the debris bed and the wall. The temperature peaking effect in the vessel wall midway between the bottom of the reactor and the top of the debris bed is due to the localized heating of the wall by the hot debris material (2500 K). The wall nodes located near the bottom of the reactor are isolated from the hot debris bed and thus have remained relatively cool

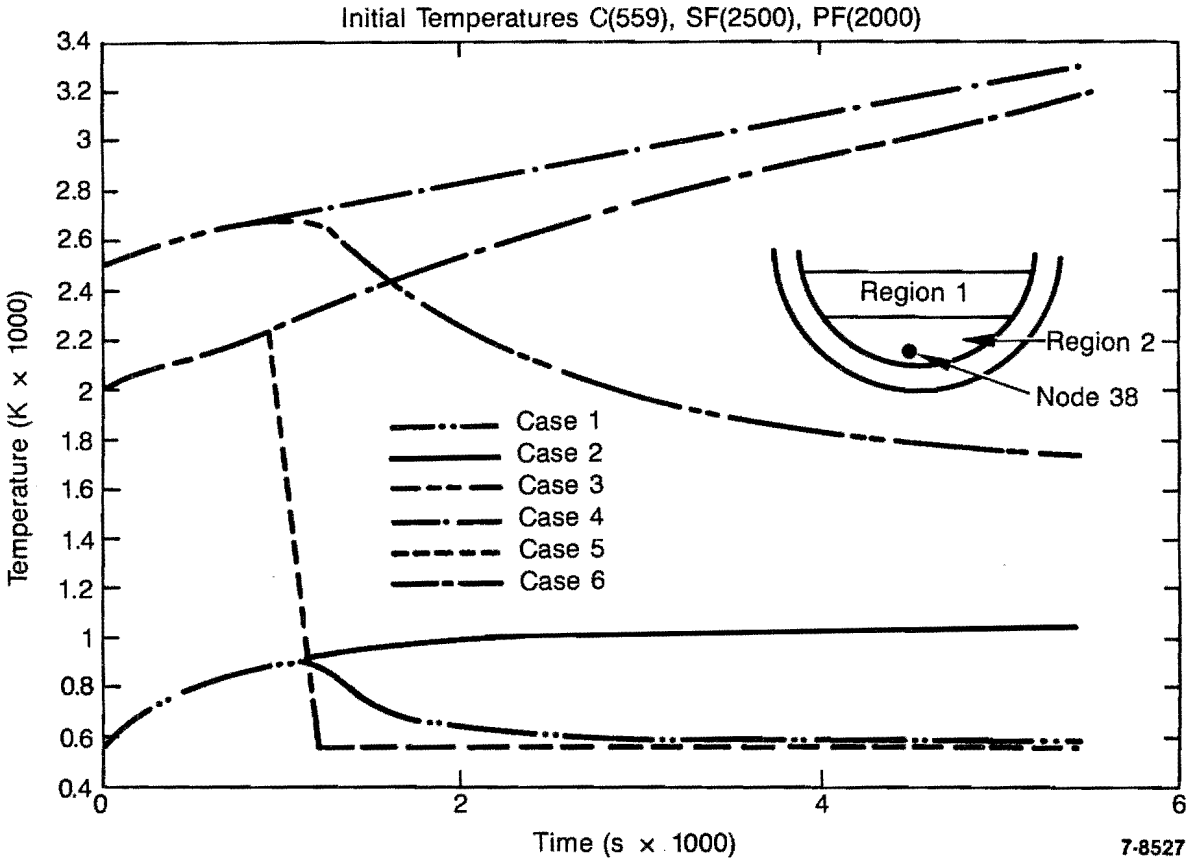

Figure 11. Temperature history of solid layer node 38.

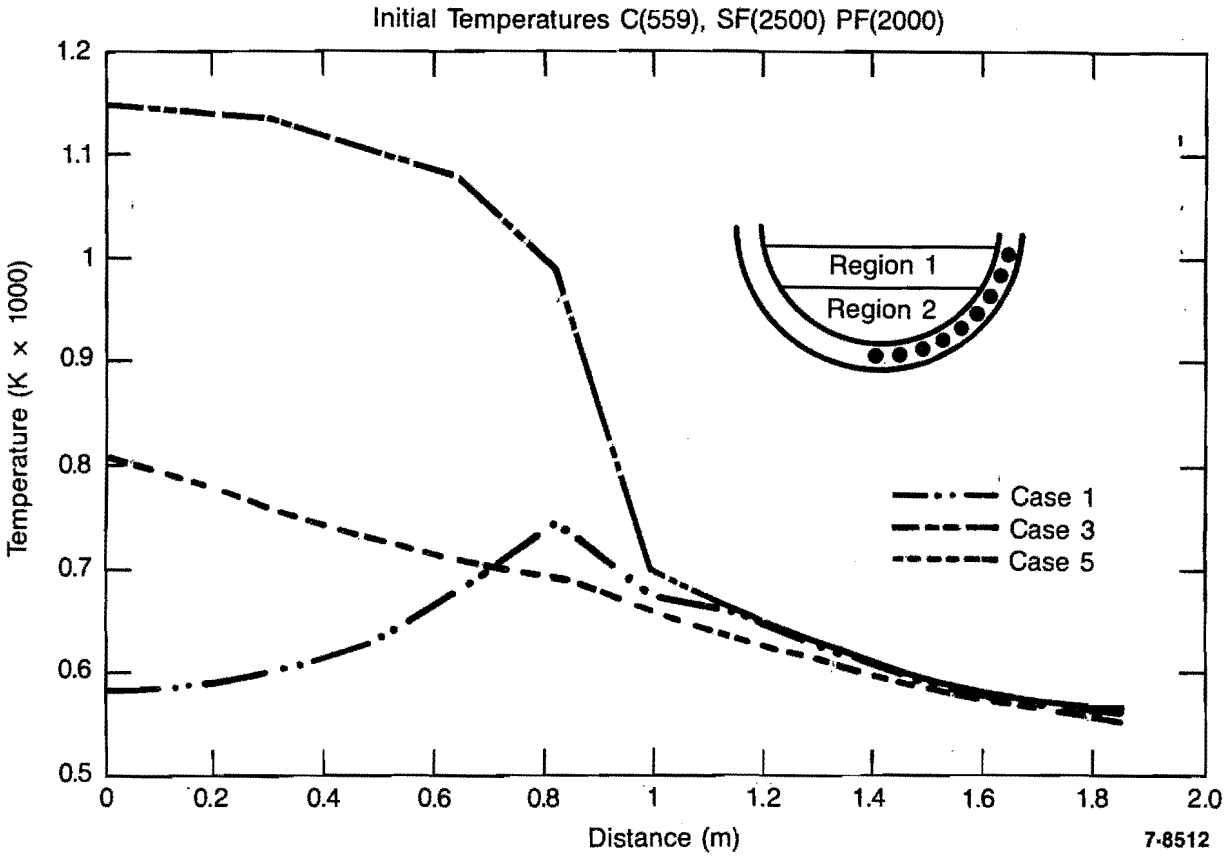

Figure 12. Mid-wall temperature profile at 1200 s into the transient (quenched cases).

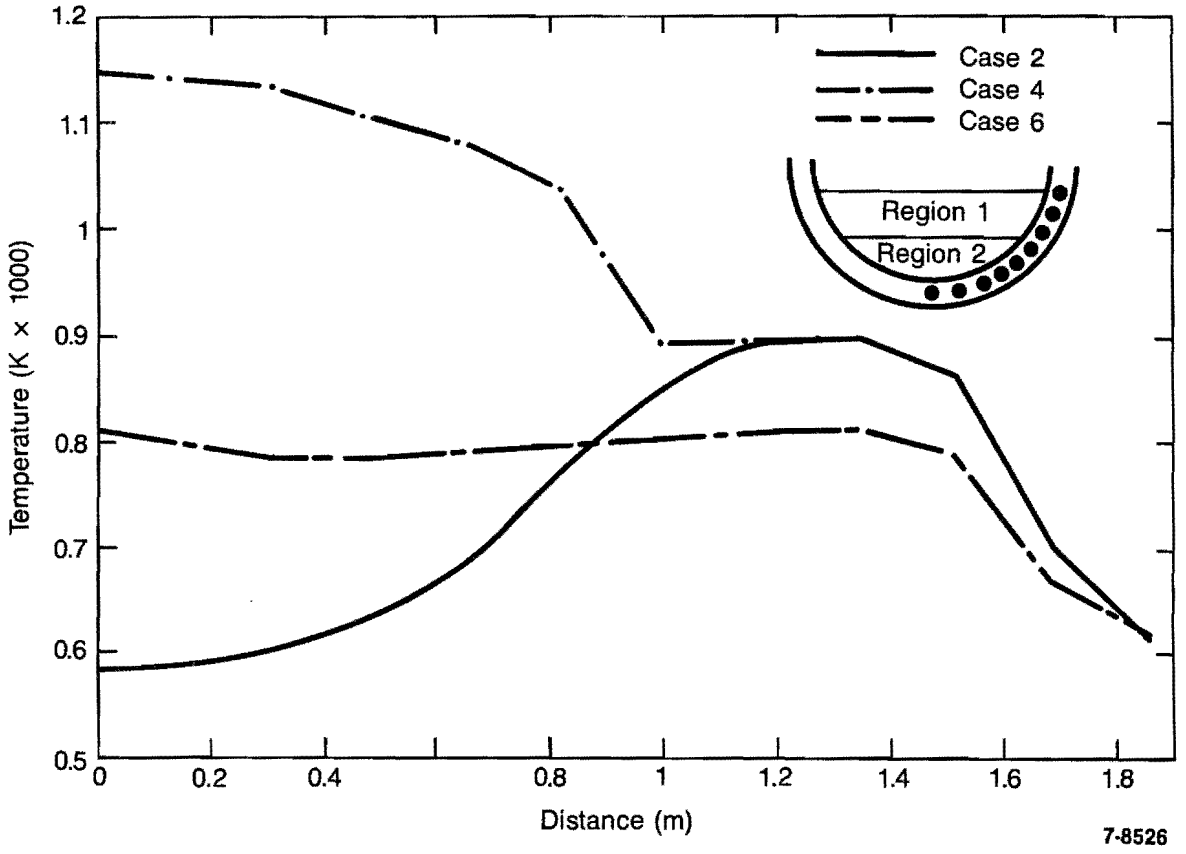

Figure 13. Mid-wall temperature profile at 1200 s into the transient (quenched cases).

during this period. The wall nodal temperature near the top of the debris bed has been influenced by the quenching action in the debris bed and is thus cooler, as indicated by the wall temperature profile.

The temperature profile for the solid fuel case shows a maximum wall temperature of 1148 K (1200 s) at the bottom of the reactor. The temperature in the wall then decreases to ~1000 K at the intersect of the wall with the porous debris bed and solid fuel material. The wall temperature then decreases sharply to 700 K. This sharp decrease in wall temperature is due to the reduced heat transfer from the porous debris bed to the wall as compared to the heat transfer from the solid fuel material to the wall. The thermal conductivity of the porous bed is less than that of the solid fuel owing to the steam-filled void in the porous material. Steam has a thermal conductivity value of ~0.14 w/m-k compared to ~6.0 w/m-k for the solid fuel region; thus, the transfer of heat from the debris bed to the vessel wall will be less that from the solid region to the wall, resulting in the temperature gradient shown in Figure 12. An additional effect on the profile is the quenching of the debris bed, which will result in cooler wall temperatures toward the top of the debris bed.

The all-porous debris bed case with quenching shows a maximum wall temperature of 809 K (1200 s) at the bottom of the reactor. The wall temperature decreases uniformly to 566 K at the top of the debris bed. This decrease is due to the quenching of the debris bed.

Figure 13 presents the same type of results for the unquenched cases. The decrease in wall temperature toward the top of the debris bed for all cases is due to assuming a quenched condition along the top of the debris bed. A summary of results presented in Figures 6 through 13, including maximum vessel wall temperatures, are presented in Table 4. The results in Table 4 show some melting (T wall >1650 K) of the inner vessel wall will occur if consolidated (internal heat generating) debris forms adjacent to the vessel wall. The melting of the inner wall occurs late in the transient (≃3000 s) resulting in the vessel wall being 30% molten at the

TABLE 4. SUMMARY OF RESULTS

Case	Peak Average Wall Temperature (K)	Time (sec)	Maximum Wall Temperature (K)	Time (sec)	Region 1 Maximum Temperature (K)	Time (sec)	Region 2 Maximum Temperature (K)	Time (sec)
1	825	680	1340	0	2833	1180	972	1180
2	1052	5400	1340	0	3794	5400	1050	5400
3	1459	5400	1701	5400	2841	1180	1936	5400
4	1518	5400	1853	5400	3982	5400	3490	5400
5	810	1160	1130	0	2391	1180	2374	1180
6	937	5400	1130	0	3527	5400	3276	5400

end of the transient (5400 s) for the most severe case, Case 4. If a high internal pressure is present, the vessel wall will likely fail, owing to creep rupture long before failure caused by a melt-through.

6. CONCLUSIONS AND RECOMMENDATIONS

The thermal response of the TMI-2 lower reactor vessel has been analyzed for three assumed lower plenum degraded core material configurations, i.e., (a) a porous debris bed resting on the vessel head, (b) a debris bed resting on top of approximately 8 inches of consolidated molten fuel adjacent to the vessel, and (c) a porous debris bed resting on top of approximately 8 inches of assumed control rod material adjacent to the vessel. For each configuration, the vessel thermal response was calculated assuming the debris was both coolable and noncoolable.

The calculations show a wide range of vessel thermal response is possible based on the debris configuration and debris cooling assumptions. Vessel melting temperatures were predicted for two of the cases (cases 3 and 4); however, for the relatively short transient (5400 s) very little melting was predicted. The most rapid heatup (resulting in the highest vessel wall temperatures) occurred for the case with assumed consolidated fuel adjacent to the vessel wall. For this case, temperatures in excess of 1100 K were achieved in less than 20 minutes and these temperatures are expected to have resulted in creep rupture during the first hour after the major core relocation. Cooling of the porous debris resting on top of the consolidated molten material had little effect on the maximum vessel temperatures for this case.

The calculations show that for a porous debris bed, vessel wall temperatures would have been sufficiently low that creep rupture of the vessel would not be expected. In addition, a layer of control rod material adjacent to the vessel wall does provide an effective insulation to the wall at locations away from the wall/fuel debris interface.

The analysis results show that the configuration of the degraded core material is crucial in estimating the vessel thermal response and ultimately the margin to failure of the vessel through mechanical analysis. The results show clearly that the configuration of the lower vessel debris material must be characterized, particularly the extent of both the loose, porous debris and the consolidated lava-like material.

Careful visual examination of the lower plenum debris should be obtained during defueling to provide sufficient detail to define the extent of the debris vs consolidated material. In addition, samples similar to the grab samples acquired from the upper core debris bed[18] should be acquired at each lower plenum inspection location (fuel assembly locations D4, D12, K9, N5 and N12) to characterize the debris material (particle size distribution, material composition and retained fission products) at several different axial locations. Several samples of consolidated material are necessary to characterize material composition and retained fission products versus material location.

7. REFERENCES

1. J. P. Adams and R. P. Smith, TMI-2 Lower Plenum Video Data Summary, EGG-TMI-7429, July 1987.

2. A. Cronenberg et al., Assessment of Damage Potential to the TMI-2 Lower Head Due to Thermal Attack by Core Debris, EGG-TMI-7222, June 1986.

3. E. L. Tolman et al., TMI-2 Accident Scenario Update, EGG-TMI-7489, December 1986.

4. P. Kuan, Core Relocation in the TMI-2 Accident, EGG-TMI-7402, November 1986.

5. E. L. Tolman et al., TMI-2 Core Bore Acquisition Summary Report, EGG-TMI-7385, September 1986.

6. R. Rainisch, Gamma Scanning of In-Core Detectors, TMI-2 Technical Planning Bulletin, April 23, 1985.

7. R. Rainisch, Analysis of Gamma Scanning of In-Core Detector No. 18 L-11 in Lower Reactor Vessel Head, GPU Nuclear Report TPO/TMI-175, June 1985.

8. L. Baker, Jr., et al., Postaccident Heat Removal Technology, ANL/RAS 77-2, January 1977.

9. E. C. Lemmon, COUPLE/FLUID, A Two-Dimensional Finite Element Thermal Conduction and Advection Code, EGG Internal Technical Report ISD-SCD-80-1, February 1980.

10. E. C. Lemmon, "Multidimensional Integral Phase Change Approximations for Finite Element Conduction Codes," Numerical Methods in Heat Transfer, John Wiley & Sons, p. 201-213, 1981.

11. P. Kuan, TMI-2 Upper-Core Particle Bed Thermal Behavior, EGG-TMI-7757, to be published.

12. "MATPRO-Version 11 (Revision 1), A Handbook of Material Properties for Use in the Analysis of Light Water Reactor Fuel Rod Behavior," NUREG/CR-0947, TREE-1280, Rev. 1 (1980).

13. J. E. Kelly, J. T Nitchevek, and M. L. Schway, "Heat Transfer Characteristic of Dry Porous Particular Beds with Internal Heat Generation," Proc. of ASME/JSME Thermal Engineering Joint Conference, Honolulu, Hawaii, Vol. 4, p. 13 (1974).

14. S. Imura and E. Takegoshi, "Effect of Gas Pressure on the Effective Thermal Conductivity of Pack Beds," Heat Transfer Japanese Research, Vol. 3, No. 4, p. 13, (1974).

15. D. Vortmeyer, "Radiation in Packed Solids," 6th Int. Heat Trans. Conf. Toronto, Canada, (1978).

16. W. J. Camp, MELPROG-PWR/MUDO: A Mechanistic Code for Analysis of Reactor Core Melt Progression and Vessel Attack under Severe Accident Conditions, SAND85-023.

17. P. Kuan, TMI-2 Core Debris Bed Coolability, EGG-TMI-7140, March 1986.

18. D. Akers et al., TMI-2 Core Debris Grab Samples--Examination and Analysis (Part 1), GEND-INF-075, September 1986.